$\delta^{13}C$ carbon isotopic composition of CO_2 in the atmosphere by Lidar. A preliminary study with a CDIAL system at 2-µm.

Fabien Gibert[1], Dimitri Edouart[1], Didier Mondelain[2], Claire Cénac[1], Camille Yver[3]

[1] Laboratoire de Météorologie Dynamique (LMD/IPSL), École polytechnique, Institut polytechnique de Paris, Sorbonne Université, École normale supérieure, PSL Research University, CNRS, École des Ponts, Palaiseau, France
[2] CNRS, LIPhy, Université Grenoble Alpes, Grenoble, France
[3] Laboratoire des Sciences du Climat et de l'Environnement (LSCE/IPSL), Unité mixte CEA-CNRS-UVSQ, UMR8212, 91191 Gif-sur-Yvette, France

Correspondence to: Fabien Gibert (gibert@lmd.polytechnique.fr)

Abstract. Our understanding of the global carbon cycle needs for new observations of CO_2 concentration at different space and time scales but also would benefit from observations of additional tracers of intra-atmospheric or surface-atmosphere exchanges to characterize sources and sinks. Lidar is a well-known promising technology for this research as it can provide, at the same time, structure of the atmosphere, dynamics and composition of several trace gas concentration. In this framework, a coherent differential absorption lidar (CDIAL) has been developed at LMD to measure simultaneously and separately $^{12}CO_2$ and $^{13}CO_2$ isotopic composition of CO_2 in the atmosphere. It also provides the radial wind speed along the line of sight of the laser. This paper investigates the methodology of three wavelengths DIAL in the spectral domain of 2-µm to obtain range-resolved CO_2 isotopic ratio $\delta^{13}C$. The set-up of the lidar as well as the signal processing is described in details. First atmospheric measurements along three days are achieved in the surface layer above the suburban area of Ecole Polytechnique campus, Palaiseau, France. Typical performances of the instrument (median values along 70h of measurement) with 10 min of time averaging show: (1) a precision around 0.6% for 1.2 km range resolution for $^{12}CO_2$ mixing ratio (2) a precision around 3.2% for 1.6 km range resolution for $^{13}CO_2$ mixing ratio. In situ co-located gas analyser measurements are used to correct for biases that are explained neither by the spectroscopic database accuracy nor the signal processing and will need further investigation. Nevertheless, this preliminary study enables to make a useful state of the art for current lidar ability to provide $\delta^{13}C$ measurements in the atmosphere with respect to geophysical expected anomalies and to predict the necessary performances of a future optimized instrument.

1 Introduction

CO_2 is the main anthropogenic greenhouse gas responsible for the current global warming. In 2024, its global annual average concentration in the atmosphere has reached more than 420 ppm and the global mean near surface temperature is 1.5 °C above the 1850-1900 average, with significant consequences for present and future life on planet Earth (WMO 2025, IPCC 2023). In our understanding of the carbon cycle, it is fundamental to associate a number of CO_2 molecules with their original surface or atmospheric sources and sinks. In particular, the biospheric sink remains very complex to assess at regional scale with current tools (bottom-up or top-down methods) given the strong ecosystem space and time heterogeneity (Friedlingstein et al., 2020). The mitigation of anthropogenic emissions needs as well other clues than a standard CO_2 mixing ratio measurement to assign a number of molecules to the type of emission: coal, gas, fuel, natural vs anthropogenic.

In this context, the CO_2 stable isotopic fraction $\delta^{13}C$ is an interesting tracer for CO_2 surface-atmosphere exchanges at local scale. It enables to characterize plant/ soil physiological processes (photosynthesis, respiration, decomposition of organic matter) and may help to issue a diagnosis on sources (anthropogenic, geological) and sinks (biosphere, ocean) of CO_2. In addition, $\delta^{13}C$ can discriminate the type of plant (C-3 or C-4) and ecosystems that contribute the most to biosphere CO_2 uptake and their evolution with warming conditions (Buchmann et al. 1998; Flanagan et al. 1996). While the difference between C3-

and C4-dominated biomes provides the largest observed variation in $\delta^{13}C$ (Still 2000), even within pure C-3 ecosystems, a large temporal and spatial variability of $\delta^{13}C$ is observed during nighttime respiration process due to species-specific effects and environmental conditions such as light, temperature and water availability, the latter being a major driver (Buchmann et al. 1997; Brugnoli et al. 1998; Bowling et al. 2002; Ekblad and Hogberg 2001; Pataki et al. 2003; Mortazavi et al. 2005). The natural variation of $\delta^{13}C$ source spreads over a scale of 100 ‰: ~ +5‰ for carbonate-gas CO_2 equilibrium in air-sea /geological water exchanges, -8‰ for standard CO_2 in the atmosphere, ~ -14‰ for C-4 plant – air exchanges but ~-27‰ for C-3 plant that is similar to fossil fuel emission (coal and oil) whereas the lowest $\delta^{13}C$ value, ~ -40‰, can be found in natural gas emission (AIEA, 2008). However, hundreds of meters from the source, these anomalies are reduced to sub 1 ‰ variations due to efficient mixing of the atmosphere (Widory and Javoy, 2003).

Concerning current instrumentation and measurement, tunable diode laser absorption (Cassidy et al. 1982) or recent cavity ring down spectroscopy (Lin et al., 2020) offer a simpler way to make in situ measurements in the atmosphere compared to former complex mass spectrometry systems (Li et al., 2018). To increase the spatial scale representativity of in situ measurement, an integrated path differential absorption (IPDA) lidar concept at 4.4 µm has also been studied (Shi et al., 2022). Although such system seems to reach similar precision on $\delta^{13}C$ (< 0.2 ‰) than in situ sensor, the horizontal profiling and 2-D mapping of $\delta^{13}C$ field above the surface by Lidar will bring new information on the patterns and origins of sources and sinks. Moreover, the vertical profiling will help characterize the local and long-distance transport of CO_2, in a similar way than Lidar measurements of water vapor stable isotopologues do already (Hamperl et al. 2022). However, 1 ‰ precision with hundreds of meters range resolution has not yet been reached for CO_2 DIAL system. Ultimately, the capability of $^{13}CO_2$ lidar measurements opens the way to a global monitoring of $^{13}CO_2$ from space using the IPDA technique to improve future global carbon inversion systems (Chen et al. 2017).

Several lidar teams have been interested in measuring CO_2 absorption with DIAL systems since almost twenty years with precursor work using DIAL systems in the 2 µm spectral band and coherent detection (Koch et al. 2004, Gibert et al. 2006) and more recent works (Gibert et al. 2015) reaching a precision of 0.5% with 150-m and 15-min range and time resolution, respectively, close to what is needed for $\delta^{13}C$ observations. The spectral band of 1.6 µm has also been considered with coherent DIAL (Yu et al. 2024) or direct detection DIAL, using the advantage of low noise internally amplified photodetector (Shibata et al. 2017; Yue et al. 2022; Stroud et al. 2023) although the obtained precision was limited by the ten times lower CO_2 absorption optical depth at such wavelength.

In this framework, a new three wavelengths coherent differential absorption Lidar (CDIAL) at 2 µm has been considered and recently developed at LMD to measure simultaneously $^{12}CO_2$ and $^{13}CO_2$ absorptions (Gibert et al. 2024). The purpose of this paper is to assess the current performances of the CDIAL system. The first sections describe the methodology and the spectral domain that has been chosen for this study. Then, a following section presents the experimental set-up, especially the new hybrid fibered/bulk laser source that was developed for this application. The signal processing is described in details to get the first lidar measurements of $^{12}CO_2$ and $^{13}CO_2$ mixing ratio. Current statistical and systematic errors are estimated. A discussion follows where the current performances of $\delta^{13}C$ are compared to useful geophysical signals to be measured in the atmosphere. Some guidelines for $\delta^{13}C$ efficient lidar measurements are pointed out.

2 Methodology

2.1 Multiwavelength DIAL theory

To measure the carbon isotopic ratio with the DIAL technique, at least three wavelengths have to be used, one serving as a reference, ideally located in a free-absorption spectral window. The differential absorption coefficients, $\alpha_{i,exp}$, measured at the different wavelengths, are estimated with the mean range gate lidar backscattered signal power, P_i, as follows:

2

$$\alpha_{i,exp} = \frac{d\tau_{i,exp}}{dR} = \frac{d}{dR}\left[-\frac{1}{2}ln\left(\frac{P_i}{P_0}\right)\right] \tag{1}$$

where $i = 1,2$ stands for $^{12}CO_2$ and $^{13}CO_2$ wavelengths respectively and $i = 0$ for the reference non-absorbed laser wavelength. $\tau_{i,exp}$ is the measured single path differential absorption optical depth (DAOD). Note that time and space averaging act at different scales in Eq. (1) that will be described later in the dedicated section on signal processing with biases and statistical error analysis. At this point, we just assume: (i) the laser wavelengths are closed enough that aerosol extinction and backscatter variations with wavelength are negligible and (2) the absorption variation is negligible in the range gate used to measure P_i.

The differential absorption coefficients are linked to the trace gas mixing ratios with:

$$\begin{pmatrix} \alpha_{1,exp} \\ \alpha_{2,exp} \end{pmatrix} = \frac{n_{air}}{(1+C_{H2O})}\begin{pmatrix} \Delta\sigma_{12C,1} & \Delta\sigma_{13C,1} & \Delta\sigma_{H2O,1} \\ \Delta\sigma_{12C,2} & \Delta\sigma_{13C,2} & \Delta\sigma_{H2O,2} \end{pmatrix}\begin{pmatrix} C_{12} \\ C_{13} \\ C_{H2O} \end{pmatrix} \tag{2}$$

where $\Delta\sigma_{12C,i} = \sigma_{12C,i}-\sigma_{12C,0}$ and $\Delta\sigma_{13C,i} = \sigma_{13C,i}-\sigma_{13C,0}$ are the differential absorption cross-section (ACS), $n_{air} = p/(k_B T)$ is the air density with T and p air temperature and pressure and k_B the Boltzman constant, C_{H2O} is the water vapour mixing ratio.

$$\begin{pmatrix} C_{12} \\ C_{13} \end{pmatrix} = \frac{1+C_{H2O}}{Det.n_{air}}\begin{pmatrix} \Delta\sigma_{13C,2} & -\Delta\sigma_{13C,1} \\ -\Delta\sigma_{12C,2} & \Delta\sigma_{12C,1} \end{pmatrix}\begin{pmatrix} \alpha_1 \\ \alpha_2 \end{pmatrix} \tag{3}$$

where $Det. = \Delta\sigma_{13C,2}\Delta\sigma_{12C,1} - \Delta\sigma_{12C,2}\Delta\sigma_{13C,1}$ and where the experimental differential absorption coefficient has been corrected by the differential absorption due to H_2O:

$$\alpha_i = \alpha_{exp,i} - \alpha_{H2O,i} \tag{4}$$

where $\alpha_{H2O,i} = C_{H2O}n_{air}\left(\sigma_{H2O,i} - \sigma_{H2O,0}\right)/(1 + C_{H2O})$.

2.2 Isotopic ratio $\delta^{13}C$ measurement

The variation of isotopic ratio is measured with respect to a reference, the Vienna Pee Dee Belemnite (VPDB) isotopic ratio 0.011237:

$$\delta^{13}C = \left[\frac{\left(\frac{C_{13}}{C_{12}}\right)_{meas.}}{\left(\frac{C_{13}}{C_{12}}\right)_{VPDB}} - 1\right] \times 1000 , \tag{5}$$

Actually, a single $\delta^{13}C$ measurement brings only little information on the carbon cycle for the atmosphere has integrated the main part of $^{12}CO_2$ and $^{13}CO_2$ variations linked to surface sources and sinks. Rather, usually, many $\delta^{13}C$ measurements are needed in a so-called Keeling plot where $\delta^{13}C$ is reported as a function of the inverse of $^{12}CO_2$ mixing ratio: $\delta^{13}C = f(1/C_{12})$. The extrapolation of $\delta^{13}C$ for high value of C_{12} gives some information about the source or sink of CO_2:

$$\delta^{13}C_{source/sink} = \delta^{13}C(C_{12} \to \infty) \tag{6}$$

Therefore, the characterization of CO_2 source and sink depends not only on $^{12}CO_2$ and $^{13}CO_2$ precision DIAL measurements but also on the amplitude of $^{12}CO_2$ variations in the atmosphere. In practice, the method needs for plume detection (anthropogenic source mainly) or diurnal cycle acquisition where large variations of CO_2 usually appear that are linked to the building of a stratified nocturnal layer and the so-called rectifier effect (Ogée et al. 2003; Widory et al. 2003; Lopez et al. 2013).

3 Spectroscopy in the 2 μm band and DIAL wavelengths positioning

CO_2 absorption measurements are usually considered in the three spectral regions 1.6, 2 or 4.3 μm. The latter has been preferred in the past given its strong absorption lines (two orders of magnitude larger than at 2 μm) to obtain the highest precision to date (0.02‰ for 400 s of time averaging) on *in situ* CO_2 isotope ratio measurement with a spectroscopic technique (Nelson et al. 2008). The 1.6 μm domain has also been considered rather for technical reason (even for CO_2 DIAL measurement) although

3

the CO_2 low absorption line strength reduced the precision obtained for $\delta^{13}C$ by one order of magnitude (2‰ for 8.7s)

(Kasyutich et al. 2006). Recent in situ cavity-ring-down spectroscopy (CRDS) instrument (PICARRO G2101-i analyzer) uses

this spectra domain to obtain a precision better than 0.3‰ (5 min). The 2-μm domain offers a compromise both for the

130   absorption coefficient and the available technical tools (laser, detector) (Andreev et al. 2011). In particular, the 2.05 μm CO_2

absorption band has already been used at LMD to make horizontal CO_2 profiles in the atmospheric boundary layer with a

coherent DIAL (CDIAL) (Gibert et al. 2015). The instrument was able to make a 150 m-15 min $^{12}CO_2$ mixing ratio

measurement with a precision of 0.5% at 500 m. However, usually the $^{13}CO_2$ absorption line intensities are far lower by two

orders of magnitude (following the isotopic ratio) than the $^{12}CO_2$ lines. This entails a non-optimal DAOD ($\tau_2 \ll 1$) which

135   reduces significantly the DIAL precision (Bruneau et al. 2006).

Fortunately, in the 2.05 μm band, the $^{13}CO_2$ line intensities and then ACS are larger by one order of magnitude that mitigates,

partly, their non-optimal DAOD. Figure 1 shows ACS calculated with line intensities from HITRAN2020 database (Gordon

et al. 2022) in the 2.06-μm spectral region. These were obtained with a multispectrum fitting approach using a modified Voigt

line shape to include line mixing and quadratic speed dependence. This database has been improved for air-broadening, air-

140   pressure shift coefficients and their temperature dependence with recent CRDS lab measurements for $^{12}CO_2$ (Mondelain et al.

2023) and for $^{13}CO_2$ absorption lines (Mondelain et al. 2025) (Table 1). The residuals obtained after the multi-spectrum fit

procedure are usually lower than 0.05 % for the absorption lines considered in this study. Note that isotopologue abundances

taken from the spectroscopic database yield a $^{13}CO_2/^{12}CO_2$ isotopic ratio of 0.011235 (https://hitran.org/docs/iso-meta/) which

differs from the VPDB's one. This creates a bias of -0.18‰ in $\delta^{13}C$. Water vapor absorption lines absorption cross-sections

145   have been calculated using a Voigt line shape and HITRAN2020 database.

Using Table 1 and Figure 1, we are able to calculate typical absorption coefficient due to $^{12}CO_2$ and $^{13}CO_2$ at the chosen

wavelengths λ_1 and λ_2: ~0.75 km^{-1} and ~0.05 km^{-1} respectively. From Eq. (1), the relative error of DIAL absorption

measurement can be roughly written $\sigma(\alpha_i)/\alpha_i \propto 1/(\alpha_i.\delta R.SNR_i)$ where SNR_i is the λ_i lidar signal to noise ratio. Therefore,

to obtain similar precision on DIAL absorption measurement at λ_1 and λ_2, $SNR_2 > 15\ SNR_1$ which represents a huge

150   instrumental effort. Comparing to Gibert et al. (2015) CDIAL set-up used for $^{12}CO_2$ measurement only, range and time

resolution will have then to be reduced and the laser should run at higher pulse repetition frequency to obtain a larger SNR.
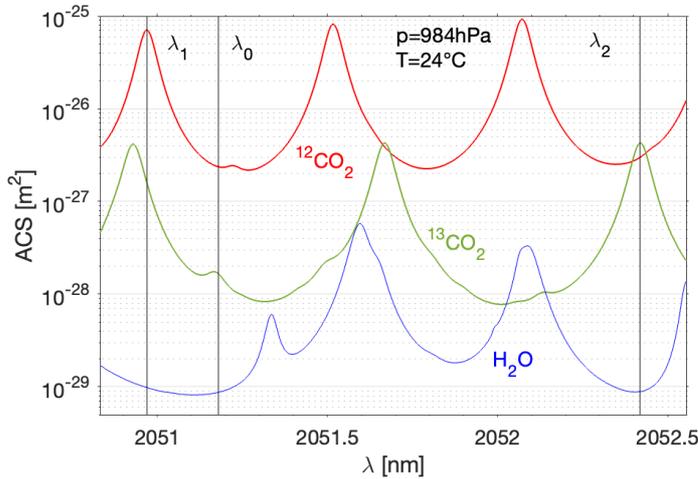

Figure 1: Absorption cross-section (ACS) for $^{12}CO_2$, $^{13}CO_2$ and H_2O for pressure 984 hPa and temperature 24°C (Voigt profile).
Isotopic ratio is taken into account. The DIAL wavelengths chosen in this work are indicated.

4

Table 1: Main $^{12}CO_2$ and $^{13}CO_2$ absorption line parameters used in this study. S: line intensity at 296 K weighted by standard isotopic abundance; E": lower energy level of the transition; γ_0 :air broadening coefficient at 296 K; $n_{\gamma 0}$: temperature dependence exponent; δ_0 :air-pressure shift coefficient at 296 K. Line intensity values and uncertainties are taken from HITRAN2020 database (Gordon et al. 2022). Values and uncertainties for γ_0 , $n_{\gamma 0}$, δ_0 are from Mondelain et al. (2023, 2025). One-sigma uncertainties are given in parenthesis in the unit of the last digit.

	ν (cm^{-1})	λ (nm)	S (cm/molecule)	E" (cm^{-1})	γ_0 (m^{-1} atm^{-1})	$n_{\gamma 0}$	δ_0 (m^{-1} atm^{-1})
$^{12}CO_2$ R30	4875.7487	2050.9670	1.510 x 10^{-22} (0.1-1%)	362.7882	6.890(2)	0.744(3)	-0.520(1)
$^{12}CO_2$ R24	4871.7917	2052.6329	2.225 x 10^{-22} (0.1-1%)	234.0833	7.049(2)	0.738(3)	-0.493(2)
$^{13}CO_2$ P18	4872.3027	2052.4176	9.59 x 10^{-24} (1-2%)	133.4456	7.360(7)	0.700(4)	-0.527(2)
$^{13}CO_2$ P14	4875.8434	2050.9272	9.58 x 10^{-24} (1-2%)	81.9440	7.649(6)	0.69	-0.510(2)

4 Experimental set-up

The lidar set-up is displayed in Figure 2 and the technical specifications are gathered in Table 2. The laser set-up has been significantly modified since our DIAL CO_2 measurements (Gibert et al. 2015, 2018) following recent work on hybrid fiber/bulk amplifier in the 2 µm domain (Lahyani et al. 2020, 2024). Our current emitter uses a seeder module with three narrow linewidth external cavity laser diodes (special model CHEETAH from Sacher Lasertechnik). Both seeders, λ_1 and λ_2, are locked to $^{12}CO_2$ and $^{13}CO_2$ absorption line centers using two frequency reference systems (FRS) built with a 80-cm path gas cell filled with pure $^{12}CO_2$ at 20 hPa and $^{13}CO_2$ at 5 hPa respectively and a Pound-Drever-Hall (PDH) technique. Gas cell pressures have been chosen to have the narrowest line shape as possible while maintaining a transmission around 0.5. λ_0 is locked to λ_1 using a phase-locking loop and a beat frequency monitoring. The spectral precision of each wavelength presents an Allan deviation better than 1 MHz between 10 s and 10 min (Gibert et al. 2018). In addition, the accuracy of each wavelength is within 1 MHz.

After a 4x1 double stage fibered switch (Agiltron) (measured cross-talk isolation larger than 45 dB), the seeder power is amplified through a CW Thulium doped fiber amplifier (TDFA) (model CTFA from Keopsys). The laser pulses are then shaped using an acousto-optic modulator AOM (model Brimrose – 50 MHz). An electro-optical modulator and a double-stage optical fibered-coupled switch (Agiltron – not represented in Fig. 2) is added to reject (by 50 dB) the long settling time CW power after the pulse. The pulse repetition rate is 6 kHz as a compromise to have a large number of samples and keep a sufficient Carrier to Noise Ratio (CNR). The wavelength switch is fixed at 60 Hz (switch every 100 pulses at fixed wavelength) as a compromise to limit switch disturbance on the measurements (switch cross-talk is limited to 30 dB) and keep identical atmospheric aerosol backscatter signal for the three wavelengths.

A custom Holmium pulsed fibered amplifier (model THALYS-2051nm-0.2W from Cybel) enables to deliver a maximum of 17 W peak power (~ 5 µJ for a 300 ns pulse duration) without parasitic stimulated Brillouin scattering (SBS) effect. The laser pulses are then amplified in a free space multi-pass Ho:YLF amplifier. Six 0.5%-Holmium doped 50-mm long Ho:YLF rods pumped by two 50-W linearly polarized Thulium fiber lasers (model TLR-50-1940-LP from IPG Photonics) are used to obtain a mean 27 W output power at 2.05 µm (4.5 mJ @ 6 kHz). Both high cross-talk isolation from the double stage optical switch and high side mode suppression from the amplifiers (Lahyani et al. 2024) give an overall spectral purity larger than 45 dB. This laser architecture enables flexible characteristics of the laser: pulse duration, energy and repetition frequency (PRF). A coherent detection with a 50-mm diameter aperture lens (optimal heterodyne efficiency for horizontal measurement close to the surface over a distance of 2 km), a balanced extended InGaAs photodiode detection (Discovery Semiconductors Inc.) and a four channels data acquisition and real time signal processing system (model Waverider-250 from LICEL) completes the set-up.
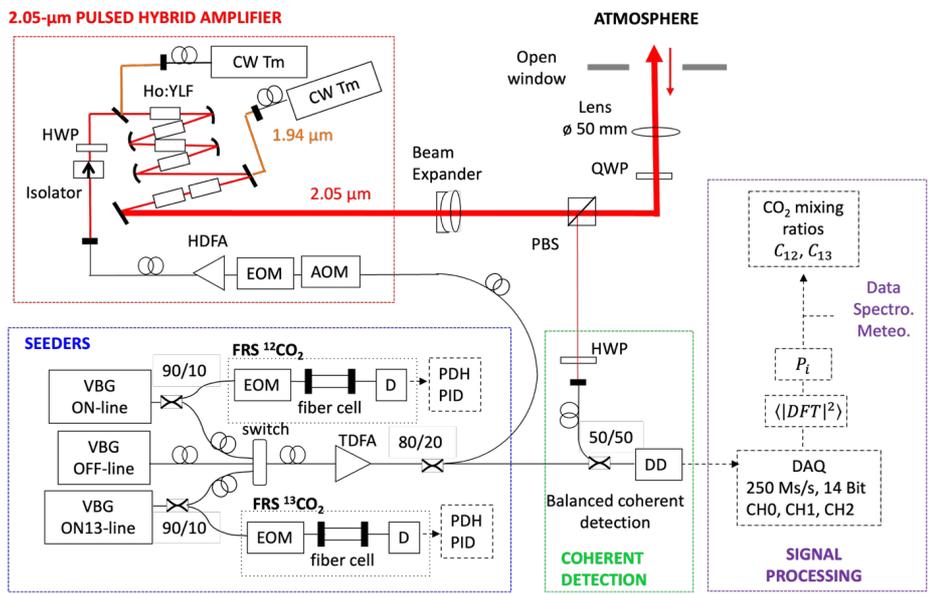
Figure 2: DIAL set-up for δ¹³C measurement. FRS : frequency reference system, EOM et AOM : electro and acoustic-optical modulators, HDFA and TDFA : Holmium and Thulium fiber amplifiers, VBG :volume Bragg grated laser diode, PDH : Pound-Drever-Hall, HWP and QWP :half and quarter wave plate, PBS : polarizer beam splitter. Signal processing: data acquisition system (DAQ) with 3 channels (CH0, CH1 and CH2) for the 3 wavelengths, real time range-gate Discrete Fourier Transform (DFT), backscatter power (P_i) at each wavelength and $^{12}CO_2$ (C_{12}) and $^{13}CO_2$ (C_{13}) mixing ratios computed with additional spectroscopic and in situ meteorological data.

Table 2: Key specifications of $^{12}CO_2$ and $^{13}CO_2$ DIAL system. Further details may be found in Gibert et al. 2018, Lahyani et al. 2020 and 2024.

Transmitter		Receiver	
Pulse energy	4.5 mJ	Lens aperture	50 mm
Pulse duration	300 ns	LOS elevation	1.4°
PRF	Shot: 6 kHz, Wavelength switch: 60 Hz	Detection Data acquisition system	Extended InGaAs PIN balanced LICEL waverider 4 channels/triggers 250 MHz 14 bit
Wavelengths	Ref. (λ_0) 2051.25 nm $^{12}CO_2$ (λ_1) 2050.97 nm $^{13}CO_2$ (λ_2) 2052.42 nm	Signal Processing	Real time 256-ns time gate (38.4-m range gate) Discrete Fourier Transform (DFT) spectrum accumulated over 1-s (2000 shots); Post-processing with Matlab software squarer and Levin estimators
Spectral stability	< 1 MHz at 10 min		
Spectral purity	> 45dB		

The lidar has been installed on the second floor of the LMD building on Ecole Polytechnique campus (10 m height above the ground). The laser beam is sent quasi-horizontally into the atmosphere through an open window. A CRDS isotope and gas concentration analyser (PICARRO model G2131-i) made simultaneous continuous measurements of $^{12}CO_2$ and $^{13}CO_2$ mixing ratios. To complete the dataset, especially to compute the spectroscopic data, meteorological data were collected at the same height of the LMD lab 200 m away.

5 Atmospheric measurements

5.1 Absorption coefficient estimates

The signal processing is similar to the one described in Gibert et al. (2015). Real time processing consists in a 256-ns time gate (38.4-m range gate) Discrete Fourier Transform accumulation over 1 s (2000 shot averaging for each wavelength). Post-

6

processing uses Matlab software with Squarer and Levin-like estimators to deliver atmospheric backscattered signal power and frequency at each wavelength (Gibert et al. 2006). The Doppler frequency shift is used to infer the radial wind speed at each wavelength (Gibert et al. 2015). Typical lidar profiles averaged over 10 min are displayed in Figure 3.
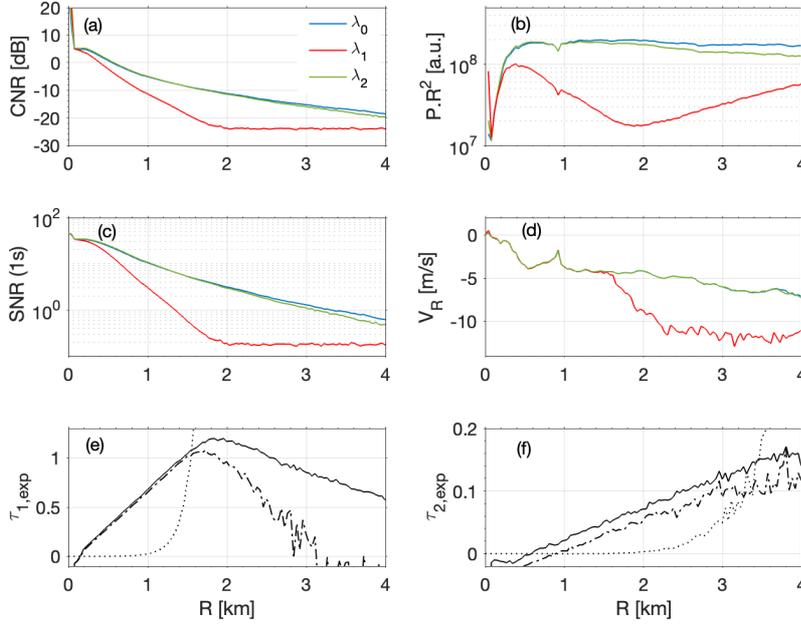
Figure 3: (a) Carrier to Noise Ratio (CNR) at each wavelength (b) Range-corrected signal (c) Signal to Noise Ratio for 1 s (d) Radial wind speed (e) DAOD calculated with signals from Levin-like estimator (solid line) and Squarer estimator (dashed and dotted line) for (e) λ_1 and (f) λ_2. The bias on DAOD calculated with Squarer estimates is indicated with the dotted line.

The CNR, $CNR_i = (P_i - P_{i,B})/P_{i,B}$ where $P_{i,B}$ is the noise power calculated using the integral of the power spectra of the last range gate of the lidar signal, is estimated for a bandwidth of 30 MHz (Fig. 3a). From the CNR and assuming that $\delta R > c\delta t$, where δt is the pulse duration, the lidar Squarer signal to noise ratio (SNR) may be estimated using (Killinger and Menyuk 1981) (Fig. 3c):

$$SNR_i^{-1} \cong N^{-0.5}(2\delta R/(c\delta t))^{-0.5}(1 + CNR_i^{-1}) \qquad (7)$$

where N is the number of averaged spectrum (number of shots) at a given distance R.

A useful estimate of statistical and systematic error of DAOD (and then absorption) can be written from the SNR (Bosenberg, 1998; Gibert et al. 2008):

$$std(\tau_{i,exp}) = (SNR_i^{-2} + SNR_0^{-2})^{-0.5}/2 \qquad (8)$$

$$\delta(\tau_{i,exp}) = (SNR_0^{-2} - SNR_i^{-2})/4 \qquad (9)$$

Figure 3f shows that the fluctuations on DAOD seems to be far larger for $\tau_{2,exp}$ ($^{13}CO_2$). The reason is that the relative error of $\tau_{2,exp}$, being proportional to the optical depth, is larger by one order of magnitude compared to $\tau_{1,exp}$, despite a larger SNR_i. Figures 3e and 3f also show that when the CNR and then the SNR decreases, the calculated DAOD is biased and underestimated as predicted by Eq. (9). Note that Levin-like estimator, which is actually used in this study, is significantly less sensitive to this bias and allows a longer range of measurement (Gibert et al. 2006).
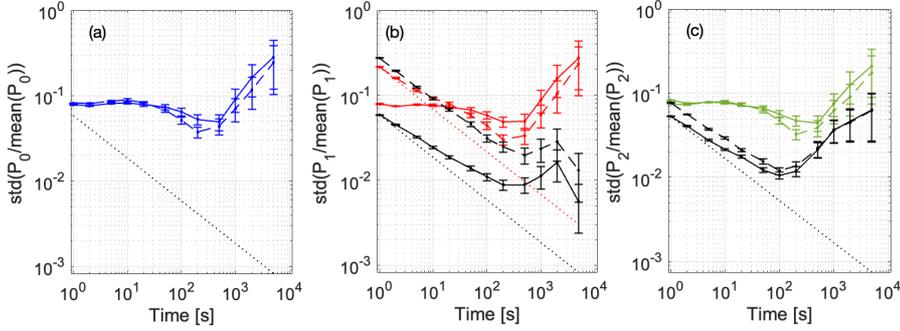
Figure 4: Allan deviation at R=0.5 km (solid line) and R=1.5 km (dashed line) for (a) λ_0 (b) λ_1 (red) and P_1/P_0 ratio (black), (c) λ_2 (green) and P_2/P_0 ratio (black). The dotted lines are indicated for the standard white noise deviation ($1/\sqrt{Time}$)

265   To optimize the statistical error reduction on the DAOD, we look at the Allan deviation of each signal power at 500 and 1500 m and of the ratios P_i/P_0 (Fig. 4). The lidar signal deviation at each wavelength does not decreases as the square root of time averaging except for very low CNR (CNR< -15 dB), i.e. for P_1 deviation at R=1.5 km (Fig. 4b). The averaged lidar signal fluctuations are mainly due to the atmosphere. The Allan deviation of the ratios P_i/P_0 shows that these fluctuations are correlated at each wavelength and their deviation decreases almost as the square root of the averaging time (but not entirely

270   suggesting that some uncorrelated noise remains) and caps at few minutes of time averaging. Therefore, in this study, the signal processing consists in averaging the ratios of 1-s lidar signals up to 10 min and then take the logarithm in Eq. (1). The distance of useful DAOD measurement is chosen to have a negligible bias from Eq. (9). The bias due to potential negative values in the logarithm is also negligible with this process (Tellier et al. 2018). Note that the usual signal processing which consists to average the signals first up to 10 min and then take the ratio and the logarithm entails an increase of the DAOD

275   standard deviation by a factor around two.

The differential absorption coefficients, $\alpha_{i,exp}$, are obtained with a Matlab bisquare linear fit on the DAOD which limits the weight of outliers with respect to the fitted line (Fig. 5). The regression is made over a distance of 1.3 km for $\alpha_{1,exp}$ ($^{12}CO_2$) and 1.8 km for $\alpha_{2,exp}$ ($^{13}CO_2$) while respecting several conditions: 1) the first points (R< 300 m) that are biased due to parasitic received CW emitted power after the emitted pulse (due to a roughly 1-μs long settling time of the AOM and switch) are

280   discarded, 2) the farthest points that are biased due to low SNR (especially for λ_1) are also discarded, 3) a reasonable larger number of points for λ_2 ($^{13}CO_2$) than for λ_1 ($^{12}CO_2$) is used to mitigate the large statistical error of $\alpha_{2,exp}$ (due to lower optical depth) while keeping the same air mass (varying number of points have been tested to give credit to this hypothesis).

a supprimé: We suspect that non-random and non-correlated fluctuations between P_i and P_0 remains (suspected from detection noise and signal processing) and will need further investigation in the future. …

a supprimé: error on
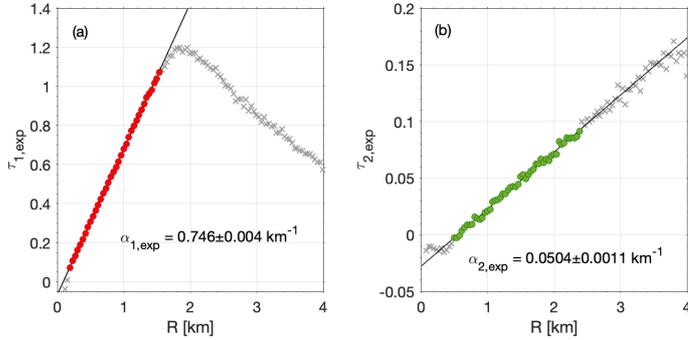
Figure 5: Differential optical depth for (a) λ_1 ($^{12}CO_2$) and (b) λ_2 ($^{13}CO_2$) and typical bisquare linear fit to estimate mean differential absorption coefficient. Colored dotted markers: points used for the fit; cross markers: outliers.

Given the error of C_{13} absorption coefficient no range-resolved measurement is tested here at higher resolution, i.e. 200 m – 10 min as such processing will only give noisy data where large CO_2 source will be hardly identified. Note anyway that range-resolved measurement for C_{12} has been tested and gives similar results as in Gibert et al. (2015). Rather here, our goal is to get a useful precision on C_{13} that will enables us to make a comparison with in situ data. Figure 5 shows an example of mean differential absorption coefficients estimates. With such conditions, the precisions on $\alpha_{1,exp}$ and $\alpha_{2,exp}$ are around 0.5% and 2%, respectively. Note that an offset spectral locking of λ_1 with respect to R30 $^{12}CO_2$ absorption line center is possible to have a similar useful distance of measurement than with λ_2, with the drawback of an increase of the statistical error though. Note also that the optical depths that we used here for CO_2 stable isotopologue measurements are similar to the ones used for DIAL H_2O stable isotopologue measurements (i.e. $H_2^{16}O$ and $HD^{16}O$) at 1.98 μm (Hamperl 2022) which enables to make some comparison in the following sections.

5.2 Meteorological data and absorption cross-section calculations

From meteorological data (p, T) and spectroscopic data we calculated the absorption cross section of each molecule ($^{12}CO_2$, $^{13}CO_2$, H_2O) at each wavelength (Fig. 6). The main differential ACS variation is observed at λ_1 and is due to temperature diurnal cycle (around 0.2% per Kelvin at R30 $^{12}CO_2$ absorption line center) (Gibert et al., 2006).
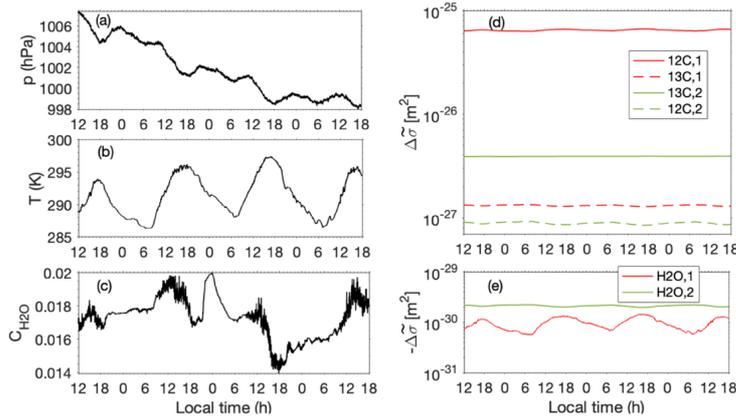
Figure 6: Meteorological data and differential ACS calculations. (a) Pressure (b) Temperature (c) H_2O mixing ratio (d) Differential ACS at wavelength 1 and 2 for $^{12}CO_2$ and $^{13}CO_2$ absorption lines and (e) for H_2O. Note that, as for Fig. 1, $^{13}CO_2$ ACS

9

a supprimé: error on

are multiplied by the VPDB isotopic ratio, i.e. 0.011237. Native in situ meteorological data have a time resolution of 1 min. Differential ACS are computed at the time resolution of Lidar measurements, i.e. 10 min.

315

5.3 Precision budget

The relative error of mixing ratio estimates results from the different parameters in Eq. (3): 1) the statistical error for absorption
320 coefficient estimates (Fig. 5) and from its correction due to H_2O absorption (Eq. (4)), 2) the uncertainty in differential ACS calculations which comes from uncertainties in meteorological data (mainly temperature) along the Lidar LOS and wavelengths position uncertainty, 3) the uncertainty in dry air density calculations mainly driven by C_{H2O} and T uncertainties along the Lidar LOS (the error due to pressure fluctuations is neglected). The relative error of each parameter is reported in Table 3. The uncertainties due to temperature fluctuations and water vapor along the line of sight of the Lidar are estimated from in situ data Allan deviation at 10 min, i.e. over the DIAL accumulation time. For the whole acquisition time (Fig. 6), the
325 Allan deviation for T and C_{H2O} is respectively 0.18 K (< 0.07 %) and 1.3 10^{-4} (< 0.9 %). These mean relative errors are used to estimate the errors of differential ACS assuming a Lorentzian absorption line shape and on the dry air density. Note that the relative error of mixing ratio due to temperature fluctuations in Table 3 accounts both from the differential ACS and the air density (Gibert at al. 2008). The relative error of α_i and then on mixing ratios due to water vapor absorption correction (Eq. 4) is calculated using an upper bound for water vapor absorption contribution in $\alpha_{i,exp}$ from Fig. 6, which amounts to 0.1 % of
330 $\alpha_{1,exp}$ and 1.7 % of $\alpha_{2,exp}$.

Table 3: Statistical errors of $^{12}CO_2$ (C_{12}) and $^{13}CO_2$ (C_{13}) mixing ratios.

Parameter	Uncertainty (%)	Comment	Reference
CO_2 absorption estimates $\alpha_{1,exp}$ $\alpha_{2,exp}$	0.6 3.2	Resolution: 1.2 km – 10 min Resolution: 1.6km – 10 min	Fig. 5
H_2O absorption correction $\alpha_{H2O,1}$ $\alpha_{H2O,2}$	< 0.0009 < 0.015	From in situ Allan deviation of C_{H2O} at 10 min. Overestimated considering an upper bound of H_2O absorption contribution in $\alpha_{i,exp}$	Fig. 6 and Eq. (4)
Differential ACS: Laser wavelength positioning	< 0.0001	Overestimated, assuming a wavelength position at absorption line center (R30 (C_{12}) and P18 (C_{13}) absorption lines) and 1 MHz frequency jitter.	Gibert et al. 2018
Temperature	< 0.01 (C_{12}) < 0.08 (C_{13})	From in situ Allan deviation of T at 10 min. Overestimated with calculations at R30 (C_{12}) and P18 (C_{13}) absorption line centers and including both absorption line intensity and air density fluctuations.	Gibert et al. 2008. Appendix B
Dry air density: Water vapor	< 0.02	From in situ Allan deviation of C_{H2O} at 10 min	Gibert et al. 2008. Appendix B

10

340 Table 3 shows that the uncertainty on mixing ratio estimates is mainly driven by the statistical error for absorption coefficient estimates from lidar backscatter signals. $^{13}CO_2$ mixing ratio estimate is also more sensitive to 1) water absorption correction due to a smaller absorption optical depth at wavelength 2 and 2) temperature fluctuations due to a less adapted energy level of the P18 transition than for $^{12}CO_2$ mixing ratio estimate. Although the DIAL system used for water vapor isotopologue measurements in Hamperl et al. (2022) is very different (direct detection DIAL), similar uncertainties were obtained for

345 absorption coefficient estimates, i.e. 0.5 % for H_2O and 2.0% for HDO for a time and space resolution of 25 min and 600 m at a mean distance of 400 m, showing that the measurement performances are driven, in both experiments, by the lowest optical depth of the stable isotopologues. However, a main difference of the two experiments concerns the spectral characteristics of the 2 µm emitters as the wavelength position precision contributes significantly in the error budget in Hamperl et al. (2022) whereas it has a negligible impact in our case.

350

5.4 Accuracy budget

At the current point of our understanding, the systematic errors in DIAL $^{12}CO_2$ and $^{13}CO_2$ mixing ratios comes from: 1) a statistical bias that is corrected using Eq. (9), 2) approximations in the DIAL equation (Eq. (1)) which neglects spectral

355 variation of aerosol extinction and backscatter coefficients especially for λ_2 (1.2 nm gap with λ_0), 3) instrumental characteristics of the DIAL emitter such as the absolute wavelength positions and the spectral purity, 4) spectroscopic data.

Table 4: Assessment of potential systematic errors of $^{12}CO_2$ (C$_{12}$) and $^{13}CO_2$ (C$_{13}$) mixing ratios.

Parameter	Bias (%)	Comment	Reference
Aerosol scattering change with wavelengths:			
- Extinction coefficient	~ 0.0003 (λ_1) ~ 0.016 (λ_2)	With respect to absorption coefficient estimated at each wavelength. Reference is taken at λ_0.	Gibert et al. 2008. Appendix A
- Backscatter coefficient	~ 0.03 (λ_1) ~ 0.1 (λ_2)		
Differential ACS: Laser wavelength positioning	< 0.0001	Assuming a 1 MHz bias in wavelength position and a Lorentzian absorption line shape	Gibert et al. 2018
Spectral purity	< 0.003	Mainly driven by to the cross-talk (< -45dB) of the double stage switch	Lahyani et al. 2021, 2024
Spectroscopic data	0.1-1 (C$_{12}$) 1-2 (C$_{13}$)	Mainly driven by line intensity uncertainties in HITRAN2020 database	Gordon et al. 2022

360 Given the 1.2 nm wavelength difference in DIAL measurements of $^{13}CO_2$, one may wonder what is the aerosol backscatter and extinction coefficient differences over such a spectral range. This has actually been studied and quantified in Gibert et al. (2008), Appendix A. A Mie scattering code for homogeneous spherical particles (Matzler 2002) accounting for typical aerosol optical depth and size distribution in the suburban area of Palaiseau and a wide range of relative humidity showed an error of CO_2 absorption coefficient of $2 \cdot 10^{-7}$ m^{-1} from the backscatter coefficient and $2 \cdot 10^{-9}$ m^{-1} from the extinction for a wavelength

365 difference of 0.3 nm at 2.06 µm. Assuming that we can describe the wavelength dependance of extinction (and backscatter coefficient) with the Angström exponent: $\delta\alpha_i = \alpha_{p,0}\left[1 - (\lambda_0/\lambda_i)^{a^0}\right]$ (Weitkamp 2005). With an assumed suburban $a^0 \sim 1$, we obtain $\delta\alpha_1 = 1.4 \cdot 10^{-4}\alpha_{p,0}$ for $|\lambda_1 - \lambda_0| = 0.3$ nm and $\delta\alpha_2 = 5.6 \cdot 10^{-4}\alpha_{p,0}$ for $|\lambda_2 - \lambda_0| = 1.2$ nm which keeps the numbers calculated above from Gibert et al. (2008) in the same order of magnitude, i.e. $8 \cdot 10^{-7}$ m^{-1} from the backscatter and 8

10^{-9} m^{-1} from the extinction coefficients. These numbers have to be compared to typical CO$_2$ absorption coefficients α_1 (~ 7.5 10^{-4} m^{-1}) and α_2 (~5.0 10^{-5} m^{-1}) to obtain the relative biases in Table 4. Our bias estimation shows that the aerosol backscatter spectral difference could have a significant impact on ^{13}CO$_2$ mixing ratio estimates (potential bias of 0.1%) if significant aerosol gradients occur in the atmosphere (plume, boundary layer interface). Other systematic errors from the spectroscopic data and DIAL emitter have been quantified as well in Table 4.

In order to quantify the actual biases on C_{12} and C_{13} estimates, we considered the direct problem. In situ differential absorption coefficients for both wavelength 1 and 2 are computed using meteorological, spectroscopic data and in situ PICARRO G2101-i isotopic gas analyzer measurements of ^{12}CO$_2$ and ^{13}CO$_2$ mixing ratios. Figure 7 shows the comparison between lidar and in situ estimates. A 'good' (with respect to expected representativity error) correlation coefficient of 0.80 and 0.82 are calculated for α_1 and α_2, respectively. However, a linear fit shows both a different amplitude of variation and a bias that are not explained up to now, neither by the signal processing nor by the potential biases listed in Table 4. The coefficients of the linear fit remain constant within the uncertainties over the four days of measurements. These biases are likely due to the long settling time of the emitted pulse shaped by the AOM (Fig. 2). As seen in Figure 3a, a part of the emitted pulse (and the remaining power after it) is reflected by the optics after the polarizer (Fig. 2) which may create a different bias on atmospheric backscattered power at each wavelength. To pursue the analysis of the lidar measurements, especially from the statistical point of view, we decided to correct the lidar absorption coefficients by these linear fit coefficients keeping in mind that further work will be needed on lidar measurements biases.
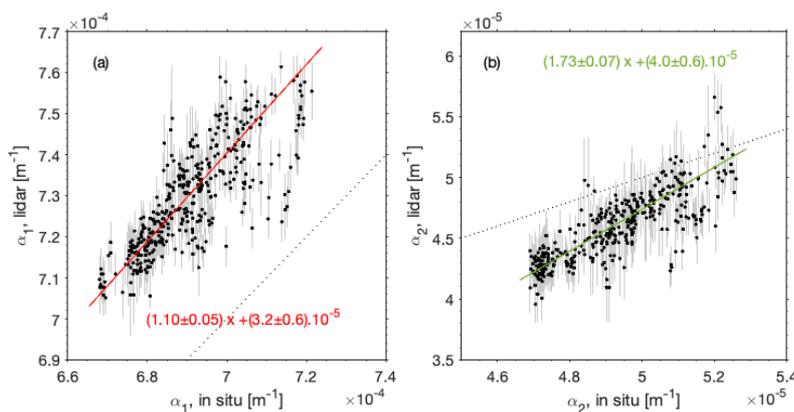

Figure 7: Comparison between lidar and in situ differential absorption coefficient (from meteorological, spectroscopic and gas analyzer data) for wavelength 1 (^{12}CO$_2$) (a) and 2 (^{13}CO$_2$) (b). The dotted line is for $\alpha_{i,lidar} = \alpha_{i,in\ situ}$.

6 Discussion

6.1 Diurnal variations of ^{12}CO$_2$ and ^{13}CO$_2$ in the atmospheric surface layer

To show the current performances of CDIAL CO$_2$ isotopic measurements, we report almost 70 h of lidar C_{12} and C_{13} mixing ratio measurements in the surface layer at approximately 15 m height above Ecole Polytechnique campus (Fig. 8). The lidar reflectivity and the radial wind speed along the line of sight (LOS) of the lidar are also displayed. The diurnal cycles of lidar C_{12} et C_{13} estimates follow the in situ data with two exceptions on 09/18 (6h) and 09/20 (10h) that correspond to changes in radial wind speed and direction (Fig.8 b and c). Large differences between in situ and lidar measurements are then explained by different spatial representativity. Other major differences are also observed on the evenings, 09/18 (20h) and 09/19 (20h). These correspond likely to anthropogenic plumes (evening road traffic) that are not well mixed during the evening transition and are located hundreds of meters far from the LMD building where is the in situ gas analyzer (R = 0 km). The ^{12}CO$_2$ anomaly

12

magnitude of these plumes (10-20 ppm) is similar to what was measured in Gibert et al. (2015). When the atmospheric boundary-layer is well mixed by turbulence (seen with fluctuated values of V_R along the LOS, 12-18 h in local time) the agreement (within the error bars) between lidar and in situ sensor measurements is excellent, as expected.

The natural change in lidar reflectivity and therefore CNR and SNR entails a variation of the maximum distance of measurements (to avoid optical depth biases) and then of the resolution of lidar differential absorption estimates along the 70 h: 1.0-1.3 km for C_{12} and 1.5-1.8 km for C_{13}. The precision of lidar mixing ratio estimates changes as well and ranges between 1.3 to 6.4 ppm for C_{12} (median value: 2.3 ppm (0.6%)) and 0.06 to 0.4 ppm for C_{13} (median value: 0.15 ppm (3.2%)).
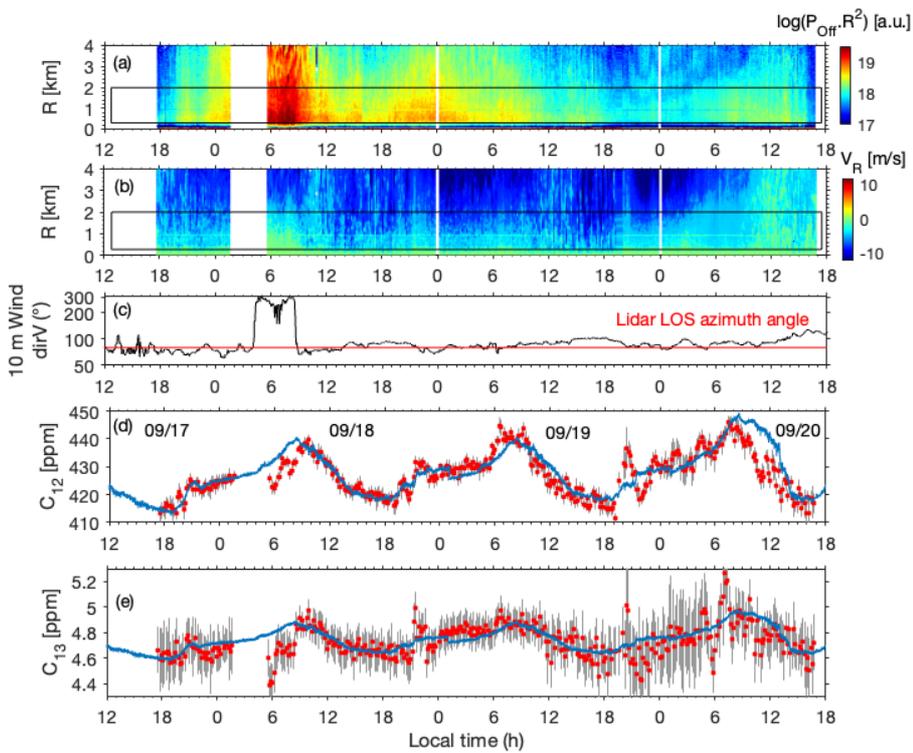
Figure 8: C_{12} and C_{13} lidar measurements. (a) Lidar reflectivity for wavelength 0 and associated (b) Lidar radial wind speed. (c) In situ horizontal wind direction (dirV) at 10 m and lidar line-of-sight (LOS) azimuth angle. (d) C_{12} and (e) C_{13} lidar mixing ratio measurements (markers). The solid line corresponds to in situ PICARRO G2101-i analyzer measurements. Space resolution for lidar C_{12} and C_{13} measurements is around 1.0-1.3 and 1.5-1.8 km respectively depending the level of the signal power (panel (a)). Time resolution is 10 min. Error bars are calculated from $\alpha_{i,exp}$ estimates (Fig. 5).

6.2 Current status and future prospective concerning δ¹³C lidar estimates

From Eq. (5), we calculated the CO_2 isotopic ratio δ¹³C both for in situ and lidar measurements and report the 70 h data in a Keeling plot (Fig. 9a). A least-squares fit on the in situ data results in a mean $\delta^{13}C_{source} = -26$ ‰ both a result of vegetation respiration and traffic road anthropogenic emissions in this suburban area (Lopez et al. 2003, Widory et al. 2003). The lidar data gave a similar value although the large uncertainty (260%) prevents us to obtain any conclusion. Using Eq. (5) we can calculate the statistical error of $\delta^{13}C$:

13

$$std(\delta^{13}C) \cong \sqrt{\frac{var(C_{12})}{c_{12}^2} + \frac{var(C_{13})}{c_{13}^2}} \qquad (10)$$

From Eq. (10) we understand that the lidar error of $\delta^{13}C$ is driven by the statistical error of C_{13} lidar mixing ratio estimate.

440 To predict the future performances of optimized lidar system for $\delta^{13}C$ measurement, we made Monte-Carlo numerical simulations assuming the same spread of $1/C_{12}$ in situ data collected during this field experiment and adding some increasing random noise on $\delta^{13}C$ in situ values. The goal was to infer an error threshold of a future optimized lidar system to see geophysical $\delta^{13}C$ sources (Fig. 9b). Typical $\delta^{13}C_{source}$ anomalies with respect to a mixed air reference of 9 ‰ have been reported on Figure 9b for comparison. The current lidar $\delta^{13}C_{source}$ error is also reported and agrees with a Monte-Carlo error

445 simulation. If we keep the same number of points that were used in this study (70 h of measurements with 10 min time resolution) we understand that a threshold lidar error should be around 7‰, 3‰, 2‰ and 1‰ to detect respectively natural gas, coal/fuel/ C-3 plant respiration, marine/geological and C-4 plant respiration $\delta^{13}C_{source}$ anomalies (Widory et al. 2003). Given that such detection should be made ideally during a single night (10 h acquisition) or for anthropogenic plumes (typical minute time scale), the precision to reach is even more challenging (< 1‰). Concerning our current lidar system, relying on a

450 coherent detection for $^{13}CO_2$ DIAL measurement, the SNR should be increased by at least 20 dB to obtain a better spatial resolution and a precision around 0.1%, which seems to be technically unreachable with the present coherent detection. However, some hope still exists with direct detection DIAL using an internally amplified photodetector such as HgCdTe avalanche photodiodes (Sun et al. 2014; Dumas et al. 2017) or superconducting nanowire single-photon detectors (SNSPD) (Yue et al. 2022).
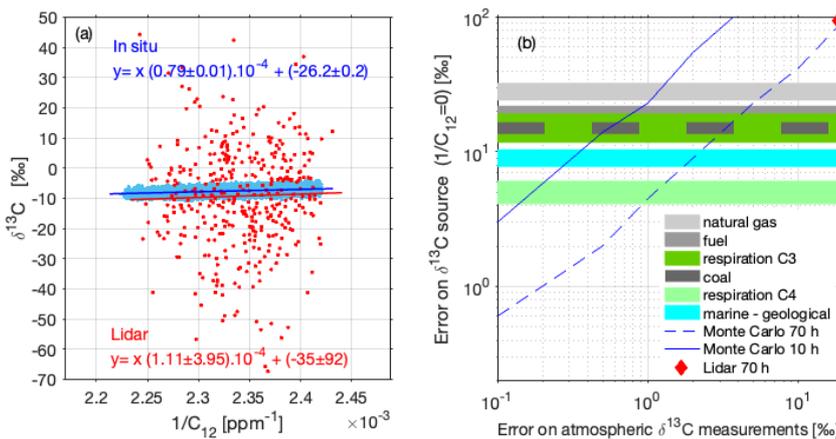
455
Figure 9: (a) Keeling plot for in situ gas analyzer and CDIAL measurements (b) Monte Carlo simulations of the $\delta^{13}C_{source}$ error estimate (time resolution is 10 min) using in situ gas analyzer as the truth and random additional noise on $\delta^{13}C$ measurements. Lidar error of $\delta^{13}C_{source}$ estimate with 70h of measurements is indicated as well as $\delta^{13}C_{source}$ geophysical typical anomalies for natural gas, fuel, coal anthropogenic emissions, C-3 and C-4 plant respiration and marine or geological source with respect to standard atmospheric mixed air $\delta^{13}C$ (9‰).
460

7 Conclusion

A first investigation of range-resolved DIAL for the measurement of CO_2 isotopic composition in the atmosphere has been
465 presented. A three wavelengths CDIAL lidar was developed for simultaneous measurements of $^{12}CO_2$ and $^{13}CO_2$ in the 2-µm spectral domain. The spectroscopic database has been updated with recent experimental data with outstanding accuracy and precision. The LMD CDIAL system has also been upgraded since 2015 and relies now on a new 27-W hybrid fiber/bulk multiple wavelength laser at 2-µm that offers similar performances but a better flexibility with respect to pulse energy, duration

14

and rate tuning. A specific optimized configuration for this study provides a three wavelengths emission with 4.5 mJ, 300 ns and 6 kHz pulses. The CDIAL system was used to make first range-resolved measurements of $^{12}CO_2$ and $^{13}CO_2$ absorption in the atmospheric surface layer above the suburban area in the south of Paris. Typical performances of the instrument (median values along 70h of measurement) with 10 min of time averaging show: (1) a precision around 0.6% for 1.2 km range resolution for $^{12}CO_2$ mixing ratio (2) a precision around 3.2% for 1.6 km range resolution for $^{13}CO_2$ mixing ratio. In situ co-located gas analyser measurements were used to correct for biases that are explained neither by the spectroscopic database accuracy nor the signal processing and will need further investigation. Then, differences in $^{12}CO_2$ and $^{13}CO_2$ mixing ratio anomalies between in situ and CDIAL made sense as the results of dynamical processes and different sounding representativity in the atmosphere. Once again, the simultaneous radial wind speed ability of the CDIAL system was critical to explain geophysical CO_2 variability in the surface layer linked to surface emissions that are not fully mixed.

Both limited precision and accuracy of the current set-up prevent us to make useful geophysical measurements of the isotopic ratio $\delta^{13}C$ in order to characterize the sources of CO_2. Nevertheless, both in situ and CDIAL measurements were used to make a state of the art for current lidar ability to provide $\delta^{13}C$ measurements in the atmosphere with respect to geophysical expected anomalies and to predict the necessary performances of a future optimized instrument. Monte-Carlo simulations showed that an increase of the instrument SNR by two orders of magnitude is necessary to get a useful geophysical precision better than 1‰ on $\delta^{13}C$. This precision is fully limited by the precision on DIAL $^{13}CO_2$ absorption measurement that suffers from a small absorption coefficient around 0.05 km^{-1} in the 2-μm spectral domain (compared to 0.75 km^{-1} for $^{12}CO_2$). Despite such increase of SNR seeming to be out of range for a coherent DIAL system with reasonable range and time resolution, such performances are still achievable with a direct detection DIAL and this will be tested in a future work.

Author contribution

FG and DE designed the DIAL system and FG carried out the experimental set-up, the atmospheric measurements and the data analysis. CC contributes to the electronics of the lidar. DM carried out the spectroscopic measurements and brought his expertise for the spectroscopic data. CY provides the in situ data for comparison. FG prepared the manuscript with contributions from all co-authors.

Competing interests

The authors declare that they have no conflict of interest.

References

Andreev, S.N., Mironchuk, E.S., Nikolaev, I.V., Ochkin, V.N., Spiridonov, M.V. and Tskhai S.N., High precision measurements of the 13CO2/12CO2 isotope ratio at atmospheric pressure in human breath using a 2-μm diode laser, Appl. Phys. B 104, 73-79, doi:10.1007/s00340-011-4602-4, 2011

Bruneau, D., Gibert, F., Flamant, P. and Pelon, J.: Complementary study of differential absorption lidar optimization in direct and heterodyne detections, Appl. Opt., 45 (20), 4898-4908, doi: 10.1364/AO.45.004898, 2006.

15

a supprimé: s

520 Buchmann, N., Kao, W.-Y., Ehleringer, J.R.,: Influence of stand structure on carbon-13 of vegetation, soils, and canopy air within deciduous and evergreen forests in Utah, United States, Oecologia, 110, 109–119, doi:10.1007/s004420050139, 1997

Buchmann, N., and J. R. Ehleringer, CO2 concentration profiles, and carbon and oxygen isotopes in C3 and C4 crop canopies, Agric. For. Meteorol., 89, 45–58, doi : 10.1016/S0168-1923(97)00059-2 ,1998

525 Bösenberg, J.: Ground-based differential absorption lidar for water-vapor and temperature profiling: methodology, Appl. Opt. 37, 3845-3860, doi: 10.1364/AO.37.003845, 1998

Bowling, D.R., McDowell, N.G., Bond B.J., Law, B.E. and Ehleringer: 13C content of ecosystem respiration is linked to
530 precipitation and vapor pressure deficit, Oecologia, 131, 113-124, doi:10.1007/s00442-001-0851-y, 2002

Brugnoli, E., Scartazza, A., Lauteri, M., Monteverdi, M.C., and Máguas C.: Carbon isotope discrimination in structural and non-structural carbohydrates in relation to productivity and adaptation to unfavourable conditions H. Griffiths (Eds) Stable Isotopes: Integration of Biological, Ecological and Geochemical Processes Bios Scientific Publishers Ltd. Oxford 133–146,
535 1998

Cassidy, D.T. and Reid, J.: Atmospheric pressure monitoring of trace gases using tunable diode lasers, Appl. Opt., 21(7), 1185-1190, doi:10.1364/AO.21.001185, 1982.

540 Chen, J. M., Mo, G., and Deng, F.: A joint global carbon inversion system using both CO_2 and $^{13}CO_2$ atmospheric concentration data, Geosci. Model Dev., 10, 1131–1156, https://doi.org/10.5194/gmd-10-1131-2017, 2017.

Dumas, D., Rothman, J., Gibert, F., Édouart, D., Lasfargues, G., Cénac, C., Le Mounier, F., Pellegrino, J., Zanatta, J.-P., Bardoux, A., Tinto, F., and Flamant, P. :Evaluation of a HgCdTe e-APD based detector for 2 μm CO2 DIAL application,
545 Appl. Opt. 56, 7577-7585, doi: 10.1364/AO.56.007577, 2017

Ekblad, A., and Högberg, P.: Natural abundance of ^{13}C in CO_2 respired from forest soils reveals speed of link between tree photosynthesis and root respiration, Oecologia, 127(3), 305-308, doi: 10.1007/s004420100667 , 2001.

550 Friedlingstein, P. et al. : Global Carbon Budget 2020, Earth Syst. Sci. Data, 12, 3269-3340, doi :10.5194/essd-12-3269-2020, 2020.

Flanagan, L. B., J. Brooks, G. T. Varney, S. C. Berry, and J. R. Ehleringer, Carbon isotope discrimination during photosynthesis and the isotope ratio of respired CO2 in boreal forest ecosystems, Global Biogeochem. Cycles, 10(4), 629–
555 640, 1996

Gibert, F., Flamant, P. H., Bruneau, D., and Loth, C.: Two-micrometer heterodyne differential absorption lidar measurements of the atmospheric CO2 mixing ratio in the boundary layer, Appl. Opt. 45, 4448-4458, doi: 10.1364/AO.45.004448, 2006

a supprimé: ¶ ... [1]

Gibert, F., Flamant, P.H., Cuesta, J., and Bruneau, D.: Vertical 2-µm Heterodyne Differential Absorption Lidar Measurements of Mean CO2 Mixing Ratio in the Troposphere. J. Atmos. Oceanic Technol., 25, 1477–1497, doi: 10.1175/2008JTECHA1070.1, 2008

Gibert, F., Edouart, D., Cénac, C., le Mounier, F. and Dumas, A., 2-µm Ho emitter-based coherent DIAL for CO2 profiling in the atmosphere, Opt. Lett. 40 (13), 3093-3096, doi: 10.1364/OL.40.003093, 2015

Gibert, F. Pellegrino, J., Edouart, D., Cénac, C., Lombard, L., Le Gouët, J., Nuns, T., Cosentino, A., Spano, P., Di Nepi, G., 2-µm double pulse single frequency Tm:fiber laser pumped Ho:YLF laser for a space-borne CO2 lidar, Appl. Opt., 57(36), 10370-10379, 2018

Gibert, F., Edouart, D., Cénac C., d13C carbon isotopic composition of CO2 in the atmosphere by Lidar. 31st International Laser Radar Conference, Landshut, Germany. (hal-04727479), Jun 2024

Gordon, I.E., L.S. Rothman, R.J. Hargreaves, R. Hashemi, E.V. Karlovets, F.M. Skinner, E.K. Conway, et al., The HITRAN2020 Molecular Spectroscopic Database, Journal of Quantitative Spectroscopy and Radiative Transfer ,277: 107949, 2022

Hamperl J., Dherbecourt, J.-B., Raybaut, M., Totems, J., Chazette, P., Régalia, L., Grouiez, B., Geyskens, N., Aouji, O., Amarouche, N., Melkonian, J.-M., Santagata, R., Godard, A., Evesque, C., Pasiskevicius, V. and Flamant, C., Range-resolved detection of boundary layer stable water vapor isotopologues using a ground-based 1.98 µm differential absorption LIDAR, Opt. Express 30, 47199-47215, 2022

IAEA, International Atomic Energy Agency: Isotopes de l'environnement dans le cycle hydrologique, IAEA-TCS-32/F, ISSN 1018-5518, Vienne, 2008

IPCC (Intergovernmental Panel on Climate Change) AR6 synthesis report : climate change, 2023

Kasyutich, V.L., Martin, P.A. and Holdsworth, R.J., An off-axis cavity-enhanced absorption spectrometer at 1605 nm for the 12CO2/13CO2 measurement, Appl. Phys. B 85, 413-420, doi: 10.1007/s00340-006-2312-0, 2006

Killinger, D.K., and Menuyk, N.: Effect of turbulence-induced correlation on laser remote sensing error, Appl. Phys. Lett., 38, 968-970, 1981

Koch G.J., Barnes, B.W., Petros, M., Beyon,J.Y., Amzajerdian, F., Yu, J., Davis, R.E., Ismail, S., Vay, S., Kavaya, M.J., and U. N. Singh: Coherent differential absorption lidar measurements of CO2, Appl. Opt. 43, 5092-5099, 2004

Lahyani, J., Le Gouët, J., Gibert, F. and Cézard, N.: 2.05 µm all-fiberlaser source designed for CO2 and wind coherent lidar measurement, Appl. Opt., 60(15), C12-C19, https://doi.org/10.1364/AO.416821, 2021.

Lahyani, J., Thiers, M., Gibert, F., Edouart, D., Le Gouët, J., and Cézard, N.: Hybrid fiber/bulk laser source designed for CO2 and wind measurements at 2.05 µm, Opt. Lett., 49 (4), 969-972, doi: 10.1364/OL.510598, 2024.

Code de champ modifié

17

Li, J., Li, R., Zhao, B.Guo, H., Zhang, S., Cheng, J. and Wu, X.,: Quantitative measurement of carbon isotopic composition in CO2 gas reservoir by micro-laser Raman spectroscopy, Spectrochim. Acta A, Mol. Biomol. Spectroc., 195, 191-198, doi:10.1016/j.saa.2018.01.082, 2018.

610 Lin, Y.-C., Zhang, Y.-L., Xie, F., Zhang, W.-Q., Fan, M.-Y., Lin, Z., Rella, C.W., and Hoffnagle J. A.: Development of a monitoring system for semicontinuous measurements of stable carbon isotope ratios in atmospheric carbonaceous aerosols: Optimized methods and application to field measurements, Anal. Chem., 92(21), 14373-14382, doi:10.1021/acs.analchem.0c02063, 2020.

615 Lopez, M., Schmidt, M., Delmotte, M., Colomb, A., Gros, V., Janssen, C., Lehman, S.J., Mondelain, D., Perrusel, O., Ramonet, M., Xueref-Remy, I. and Bousquet, P.: CO, NOx and 13CO2 as tracers for fossil fuel CO2: results from a pilot study in Paris during winter 2010, Atmos. Chem. Phys., 13, 7343-7358, doi:10.5194/acp-13-7343-2013, 2013

Mätzler, C., 2002: MATLAB functions for Mie scattering and absorption, version 2. IAP Research Rep., 11 pp.
620

Mondelain, D., Campargue, A., Fleurbaey, H., Kassi, S., Vasilchenko, S. : Line shape parameters of air-broadened 12CO2 transitions in the 2-μm region, with their temperature dependence, J. Quantitative Spectrocopy Radiative Transfer, 298, 108485, doi: 10.1016/J.jqsrt.2023.108485, 2023

625 Mondelain, D., Campargue, A., Gamache, R.R., Hartmann, J.-M., Gibert, F., Wagner, G., Birk, M., Röske C.: Isotopologue dependence of the CO2-air broadening and shifting coefficients: experimental evidence and comparison with theory for 13CO2 and 12CO2, J. Quant. Spect. Radiative Transfer, 333, 109271, doi: 10.1016/j.JQSRT.2024.109271, 2025

Mook, W.G., Koopmans, M., Carter, A.F. and Keeling, C.D.: "Seasonal, latitudinal, and secular variations in the abundance and isotopic ratios of atmospheric carbon dioxide: 1. Results from land stations". Journal of geophysical research-Oceans and atmospheres, 88(NC15), 915-933, 2014.
630

Mortazavi, B., Chanton, J.P., Prater, J.L., Oishi, A.C., Oren, R., Katul, G.: Temporal variability in (13)C of respired CO(2) in a pine and a hardwood forest subject to similar climatic conditions. Oecologia, 142(1), 57-69, doi: 10.1007/s00442-004-1692-2, 2005
635

Nelson, D.D., McManus, J.B., Herndon, S.C., Zahniser, M.S., Tuzson, B. and Emmenegger L., New method for isotopic ratio measurements of atmospheric carbon dioxide using a 4.3 μm pulsed quantum cascade laser, Appl. Phys. B 90, 301-309, doi:10.1007/s00340-007-2894-1, 2008
640

Ogée, J., Peylin, P., Ciais, P., Bariac, T., Brunet, Y., Berbigier, P., Roche, C., Richard, P., Bardoux, G., and Bonnefond, J.-M.: Partitioning net ecosystem carbon exchange into net assimilation and respiration using 13CO2 measurements: A cost-effective sampling strategy, Global Biogeochem. Cycles, 17(2), 1070, doi:10.1029/2002GB001995, 2003

645 Pataki, D.E., Ehleringer, J.R., Flanagan, L.B., Yakir, D., Bowling, D.R., Still, C.J., Buchmann, N., Kaplan, J.O., Berry, J.A.: The application and interpretation of Keeling plots in terrestrial carbon cycle research, Global Biogeochem Cycles, 17, doi: 10.1029/2001GB001850, 2001

18

Pataki, D. E. , Ehleringer, J. R. , Flanagan, L. B. , Yakir, D. , Bowling, D. R. , Still, C. J. , Buchmann, N. , Kaplan, J. O. , & Berry, J. A.:The application and interpretation of Keeling plots in terrestrial carbon cycle research. Global Biogeochemical Cycles, 17(1), 1022, doi :10.1029/2001gb001850, 2003

Shi, T., Han, G., Ma, X., Gong, W., Pei, Z., Xu, H., Qiu, R., Zhang, H. and Zhang, J.: Potential of ground-based multiwavelength differential absorption lidar to measure d13C in open detected path, IEEE Geoscience and remote sensing letters, 19, 7003204, doi: 10.1109/LGRS.2021.3130585, 2022.

Shibata, Y., Nagasawa, C. and Abo, M.: Development of 16 μm DIAL using an OPG/OPA transmitter for measuring atmospheric CO2 concentration profiles, Appl. Opt. 56(4), 1194–1201, 2017.

Sun, X., Abshire, J.B., and Beck, J.D.: HgCdTe e-APD detector arrays with single photon sensitivity for space LIDAR applications, Proc. SPIE 9114, 91140K, 2014

Still, C.J. : C-4 plants and the carbon cycle: studies at regional and global scales. PhD thesis, Stanford University, 2000

Stroud, J.R.; Wagner, G.A.; Plusquellic, D.F. Multi-Frequency Differential Absorption LIDAR (DIAL) System for Aerosol and Cloud Retrievals of CO_2/H_2O and CH_4/H_2O. Remote Sens., 15, 5595. https://doi.org/10.3390/rs15235595, 2023

Tellier, Y., Pierangelo, C., Wirth, M., Gibert, F. and Marnas, F.: Averaging bias correction for the future space-borne methane IPDA lidar mission MERLIN, Atmos. Meas. Tech., 11, 5865-5884, doi:10.5194/amt-11-5865-2018, 2018

Weitkamp C.: Lidar. Range-resolved optical remote sensing of the atmosphere, 2005.

Widory, D. and Javoy, M.: The carbon isotope composition of atmospheric CO2 in Paris, Earth and Planetary Science Letters, 215, 289-298, doi: 10.1016/S0012-821X(03)00397-2, 2003

WMO, State of the Global Climate 2024, WMO-No.1368, ISBN 978-92-63-11368-9, https://library.wmo.int/idurl/4/69455

Yu, S., Guo, K., Li, S., Han, H., Zhang, Z., and Xia, H.: Three-dimensional detection of CO2 and wind using a 1.57 μm coherent differential absorption lidar, Opt. Express 32, 21134-21148, 2024

Yue, B., Yu, S., Li, M., Wei, T., Yuan, J., Zhang, Z., Dong, J., Jiang, Y., Yang, Y., Gao, Z., et al. : Local-Scale Horizontal CO2 Flux Estimation Incorporating Differential Absorption Lidar and Coherent Doppler Wind Lidar. Remote Sens., 14, 5150, doi:10.3390/rs14205150, 2022